PAPER

(●) Check for updates

Synthesis of palm sheath derived-porous carbon for selective CO$_2$ adsorption†

Yan Zhang, (ID) *[a] Ziqi Wei,[a] Xing Liu,[b] Fan Liu,[c] Zhihong Yan,[a] Shangyong Zhou,[a] Jun Wang (ID) [b] and Shuguang Deng (ID) *[d]

Biomass-derived porous carbons are regarded as the most preferential adsorbents for CO$_2$ capture due to their well-developed textural properties, tunable porosity and low cost. Herein, novel porous carbons were facilely prepared by activation of palm sheath for the highly selective separation of CO$_2$ from gas mixtures. The textural features of carbon materials were characterized by the analysis of surface morphology and N$_2$ isotherms for textural characterization. The as-prepared carbon adsorbents possess an excellent CO$_2$ adsorption capacity of 3.48 mmol g^{-1} (298 K) and 5.28 mmol g^{-1} (273 K) at 1 bar, and outstanding IAST selectivities of CO$_2$/N$_2$, CO$_2$/CH$_4$, and CH$_4$/N$_2$ up to 32.7, 7.1 and 4.6 at 298 K and 1 bar, respectively. Also, the adsorption evaluation criteria of the vacuum swing adsorption (VSA) process, the breakthrough experiments, and the cyclic experiments have comprehensively demonstrated the palm sheath derived porous carbons as efficient adsorbents for practical applications.

1. Introduction

In the last decade, CO$_2$ emission caused by the combustion of fossil fuels has caused widespread concern in the world due to its critical role in global climate change and the energy crisis.[1–3] Efficient CO$_2$ capture and sequestration are very important to climate change mitigation, control of atmospheric pollution in confined spaces, mining safety, and the production of synthetic fuels and high-value chemicals.[4–6] Amine scrubbing was always employed to remove CO$_2$ from the exhaust gas in the traditional method. However, the inherent drawbacks of the technique, such as intensive energy consumption, corrosion of the equipment, the degradation of solvent, and potentially hazardous waste, limit its applications.[7–9] In recent years, physisorption by virtue of the pressure swing adsorption process (PSA) is regarded as an energetically efficient and reliable method to separate gases, due to its moderate operating process, the feasibility of site production, and the ability to disperse operations in remote regions. As adsorbents are crucial to the PSA process, developing novel adsorbents with large adsorption capacity and high

selectivity, featuring excellent stability and good reusability would be promising.[10,11]

In recent years, attractive solid materials, including zeolites,[12] metal–organic frameworks (MOFs),[13] coordination organic polymers,[14] and porous carbons,[15] have been evaluated. Among them, porous carbons possess the inherent merits of low cost, excellent stability, outstanding adsorption and separation ability, easy to regenerate, which have been verified to be an excellent candidate for CO$_2$ capture, the separation of CO$_2$/N$_2$,[16] CO$_2$/CH$_4$,[17,18] and CH$_4$/N$_2$ (ref. 19) binary gas mixtures. Biomass-derived porous carbons are the most promising candidate for industrial application in gas separation, due to their instinctive properties of large surface area, well-developed pore structure, controllable pore size, and chemically inert.[16] Recently, many endeavors have been used biomass for preparing activated carbons with high porosity useful for high capacity CO$_2$ adsorption. González *et al.* prepared olive stones derived carbons, and the CO$_2$ capacity was relatively low (3.0 mmol g^{-1}) at 298 K under 1 bar.[20] Singh *et al.* prepared Arundo donax-based porous carbons with a relatively low CO$_2$ capacity of 2.2 mmol g^{-1} 298 K and 1 bar.[21] Therefore, the carbon precursors and the preparation methods were of great significance for improving gas adsorption and separation performance.

Traditional activation using KOH as activator can produce well-developed pores that are conducive to CO$_2$ adsorption, which is widely used in the preparation of activated carbons.[22,23] As the structural properties of activated carbon and the amount of KOH required are related to the precursor, other biomass can be used as a carbon source to prepare effective activated carbon. Biomass feedstocks, such as palm sheath (PS) composed of

[a] Jiangxi University of Chinese Medicine, Nanchang, 330031, Jianxi, PR China. E-mail: zhangyan1987127@163.com

[b] School of Resource, Environmental and Chemical Engineering, Nanchang University, Nanchang, 330031, Jiangxi, PR China

[c] Jiangxi Province Key Laboratory of Modern Analytical Science, Nanchang University, Nanchang 330031, Jiangxi, PR China

[d] School for Engineering of Matter, Transport and Energy, Arizona State University, 551 E. Tyler Mall, Tempe, AZ 85287, USA. E-mail: shuguang.deng@asu.edu

crossed fibers with different diameters are always regarded as forest waste.[24] However, it is competitive because they are not only widely distributed, easy to regenerate, and low cost but also happen to have a large surface area by KOH activation. Unfortunately, there are few studies on the preparation of PS-derived porous carbon to improve CO_2 absorption capacity and gas separation performance.

Herein, PS-derived porous carbon was facilely prepared *via* a one-step KOH activation procedure using palm sheath as a carbon precursor. The surface area and porosity are tunable by altering the activation condition (KOH/biomass ratio or activation temperature). Moreover, the porous carbon was systematically characterized and the CO_2, CH_4, and N_2 isotherms were measured to assess the selective adsorption performance. The obtained PS-derived porous carbon exhibited an outstanding CO_2 uptake capacity and excellent CO_2/N_2, CO_2/CH_4, and CH_4/N_2 selectivity. Then, the micropores play a dominant role in the CO_2 adsorption capacity was verified at 1 bar. Furthermore, the outstanding dynamic breakthrough curves and satisfactory vacuum swing adsorption (VSA) working capacity also demonstrate that the as-prepared porous carbons are potent candidates for real-world application.

2. Materials and methods

2.1 Materials

The palm sheath (PS) used in this study was kindly provided by Arizona State University and wash off the dirt with water and dry overnight at 110 °C, then crushed to 40 mesh (<0.45 mm). Potassium hydroxide (KOH) and hydrochloric acid (HCl) were purchased from Aladdin. All chemicals were used directly without any further purification.

2.2 Preparation of palm sheath-derived porous carbon

The typical synthesis procedure of microporous PSK-*X-Y* was shown below. Firstly, crushed PS powder was mixed with aqueous KOH solution (KOH/PS = 1/1, 2/1, and 3/1 by weight ratios), dried at 110 °C for 3 h to remove the redundant aqueous solvent, then transfer the slurry to the crucible. Afterward, the slurry was heated in a tubular furnace to a target temperature of 550–750 °C at a heating rate of 10 °C min^{-1} in N_2 atmosphere and hold at this temperature for 1 h. Subsequently, the obtained sample was washed with 1 M HCl to remove inorganic salts and residue KOH. Then the solution was removed, and the porous carbon was rinsed with deionized water until neutral. Finally, the porous carbons were then dried in a vacuum oven at 80 °C for 12 h. The as-synthesized porous carbons were denoted as PSK-*X-Y*, where *X* represents the KOH/PS ratio, and *Y* denotes the activation temperature in °C. PSK-650 was prepared in the same procedure but without KOH at 650 °C for 1 h.

2.3 Material characterization and adsorption measurements

Powder X-ray diffraction (PXRD) analysis with a Bruker D8 ADVANCE XRD instrument (40 kV, 40 mA, Cu Ka = 1.5418 Å) was used to investigate the crystal structure of the activated carbons. Raman spectra were collected using an HR Evolution

Raman microscope. Scanning electron microscopy (SEM, JSM 6701F instrument) and Transmission electron microscopy (TEM, JEM-2100 apparatus) were used to analyze the morphology of the as-synthesized Palm Sheath-derived porous carbon. A CHNS elemental analyzer (Vario Micro) with an O measurement mode was used to characterize the bulk composition (carbon, hydrogen, nitrogen and oxygen) of prepared samples. X-ray photoelectron spectroscopy (XPS, Thermo, ESCALAB250Xi) was used to characterize the surface composition of prepared samples.

The Micromeritics ASAP 2460 adsorption apparatus (Micromeritic Instruments, USA) was used to measure the pure component adsorption isotherms of CO_2, CH_4, and N_2 at 273 and 298 K. All samples were degassed at 393 K for 12 h before adsorption measurements. The BET (Brunauer–Emmett–Teller) surface area was calculated using the N_2 adsorption isotherm data between 0.05 and 0.3 relative pressure at 77 K, and pore size distributions were calculated using DFT (nonlocal density functional theory) from the N_2 adsorption–desorption isotherms measured at 77 K.

The details of breakthrough experiments are shown in the ESI (Fig. S1†).

3. Result and discussion

3.1 Surface morphology and phase structure

Surface morphology of PS-derived porous carbon was investigated using scanning electron microscopy (SEM) and Transmission electron microscope (TEM) (Fig. 2). The surface morphology of all the PS-derived carbons show the presence of abundant pores which are originated due to the liberated of volatiles or decomposed components of the biomass during the activation process. The pristine PS displayed smooth surfaces without obvious pores (Fig. 1a, e). Upon treatment with KOH, the sample with smooth surface transferred into a three-dimensional framework with abundant pore and tunnel structures, which is associated with the KOH etching during the activation process (Fig. 1b). With increasing KOH/PS ratio and activation temperature, more irregular and large cavity/defects were found (Fig. 1c). After further increases in the proportion of KOH and temperature, we can see the pores collapsed (Fig. 1d). TEM images displayed that the activated samples generate numerous disordered slit-like micropores with low graphitic degrees all over the carbon (Fig. 1f–h). These results matched the result of N_2 adsorption measurement, which determine its characteristics of microporous features.

X-ray diffraction (XRD) was used to further investigate the crystal structures of as-prepared carbons, as shown in Fig. 2a. The XRD spectra of obtained porous carbons (Fig. 2a) exhibit two broad peaks centered at $2\theta \approx 23°$ and $43°$, which could be assigned to (002) and (100) reflections of graphite. Both diffraction peaks are broad and low intensity, indicating the amorphous nature of PSs with small crystalline domains.[25] With KOH amount and activation temperature increased, the intensities of these two diffraction peaks decreased, suggesting more defects produced under these conditions.[26] Two obvious bands at around 1335 cm^{-1} (D band) and 1572 cm^{-1} (G band) for three
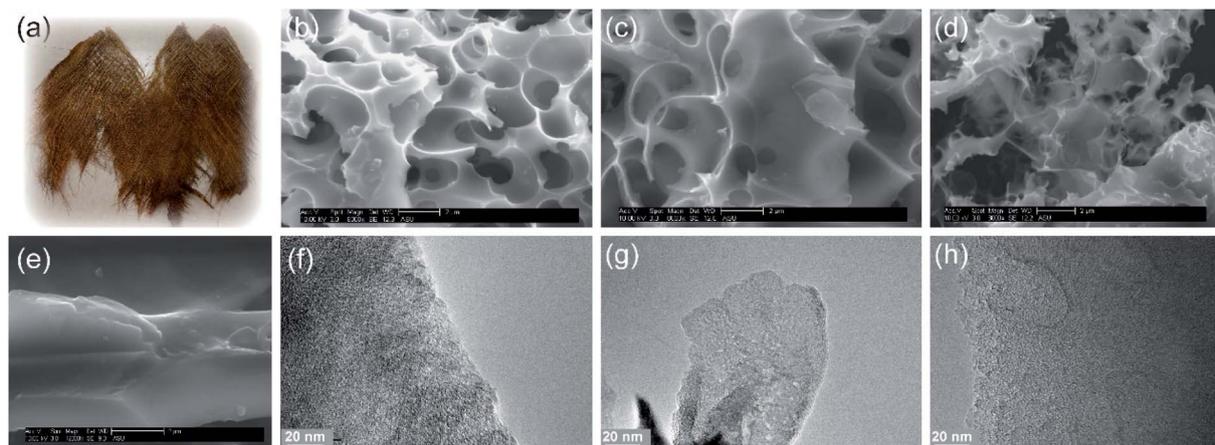
Fig. 1 (a) Palm sheath; the SEM images of (b) PSK-1-550, (c) PSK-2-650, (d) PSK-3-750, (e) PSK-650; TEM images of (f) PSK-1-550, (g) PSK-2-650, (h) PSK-3-750.

samples were observed in the Raman spectra (Fig. 2b), corresponding to the disordered/defective carbon structures and the vibration of sp²-hybridized carbon atoms in the graphitic layer, respectively.[27,28] The I_D/I_G value of PSK-1-550, PSK-2-650, and PSK-3-750 is calculated to be 0.95, 0.96, and 0.98, respectively, which represents that more defects were produced at harsh activation conditions. The formation of the layered graphene-like structure was further demonstrated with the emergency of the characteristic 2D band (at 2794 cm⁻¹) at higher temperature.[29] The

thermal stability of PS-derived carbons was investigated by TGA (Fig. 2c). The mass loss occurred around 100 °C was ascribed to the desorption of adsorbed moisture. The PS-derived carbons were thermally stable up to a temperature of 500 °C, which is more than adequate for many practical applications.

3.2 Porous properties and pore size distribution analysis

The N_2 adsorption–desorption isotherms were used to investigate the textural properties of the PS-derived carbons (Fig. 2d
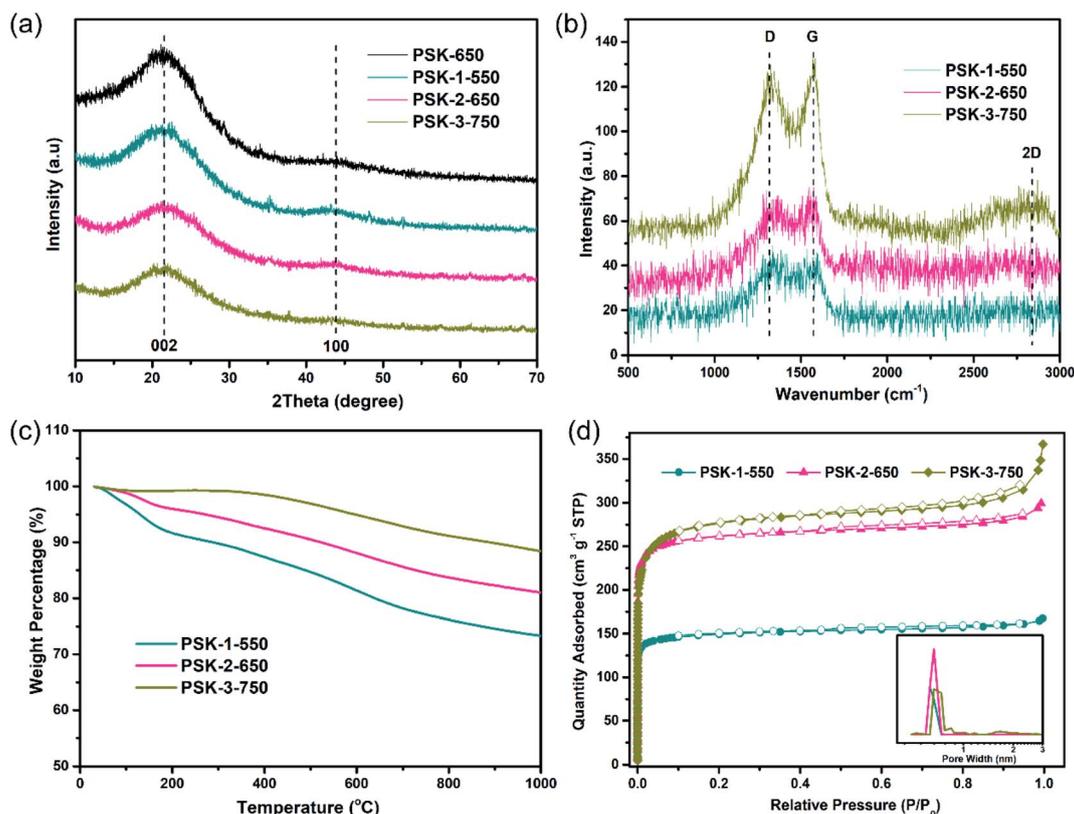

Fig. 2 (a) XRD patterns, (b) Raman spectra, (c) TGA curves and (d) N_2 isotherms.

© 2022 The Author(s). Published by the Royal Society of Chemistry

Table 1 Pore textural properties and CO_2 adsorption uptake for the PS-derived carbons

Sample	S_{BET}^{a} (m^2 g^{-1})	V_p^{b} (cm^3 g^{-1})	V_{micro}^{c} (cm^3 g^{-1})	V_n^{d} (cm^3 g^{-1})	V_0^{e} (%)	CO_2 uptake (mmol g^{-1}) 273 K, 1 bar	298 K, 1 bar	273 K, 0.15 bar	298 K, 0.15 bar	CH_4 uptake (mmol g^{-1}) 273 K, 1 bar	298 K, 1 bar
PSK-1-550	480	0.30	0.20	0.24	66%	3.35	2.70	1.63	1.02	1.62	1.02
PSK-2-650	840	0.46	0.35	0.36	76%	5.28	3.48	2.00	1.09	2.20	1.47
PSK-3-750	894	0.54	0.33	0.12	61%	4.11	2.21	1.14	0.55	1.47	0.98

[a] The specific surface area was determined by the BET equation ($P/P_0 = 0.05$–0.3). [b] Total pore volume at $P/P_0 = 0.99$. [c] The micropore volume was estimated as $d < 2$ nm using the equilibrium model for slit pores. [d] Pore volume of narrow micropores (<6.6 Å) was calculated by the NLDFT method using N_2 isotherms at 77 K. [e] Percentage of the volume of micropores in the total pore volume.

and S3†). All of the PS-derived carbons exhibited type I isotherms, with an obvious N_2 uptake at a low relative pressure ($P/P_0 < 0.01$), suggesting the presence of abundant micropores in the resulting adsorbents.[30,31] It is worth noting that the surface properties and pore volume of the materials can be controlled by the activator dosage and activation temperature. For example, the BET surface area increased from 671 m^2 g^{-1} to 840 m^2 g^{-1} with the KOH/PS ratio increase from 1 to 2 at the activation temperature of 650 °C (Fig. S3b and Table S2†). With the KOH/PS ratio further increased to 3, the BET surface area decreased to 620 m^2 g^{-1} on PSK-3-650, this phenomenon may be caused by over activation and collapse of micro/mesopores. The effect of activation temperature was also analyzed, the

BET surface area increases from 486 m^2 g^{-1} to 1052 m^2 g^{-1} with the temperature increasing from 550 °C to 750 °C at the porogen/PS ratio of 2. Moreover, the pore volume can be controlled as well, the total pore volume increased from 0.30 cm^3 g^{-1} to 0.54 cm^3 g^{-1} with the activation become harsh. Impressively, PSK-2-650 displays a moderate BET surface area of 840 m^2 g^{-1} and a total pore volume of 0.46 cm^3 g^{-1}, which has the potential to show high CO_2 selective capacity.[16,32] Thus, N_2 adsorption–desorption isotherm under ultra-low pressure was further measured to study the effect of micropores on CO_2 adsorption. As shown in Fig. 2d, ultra-micropores smaller than 10 Å was observed in PSK-1-550 and PSK-2-650, whereas partial pores above 10 Å with a small proportion of pores larger than 20
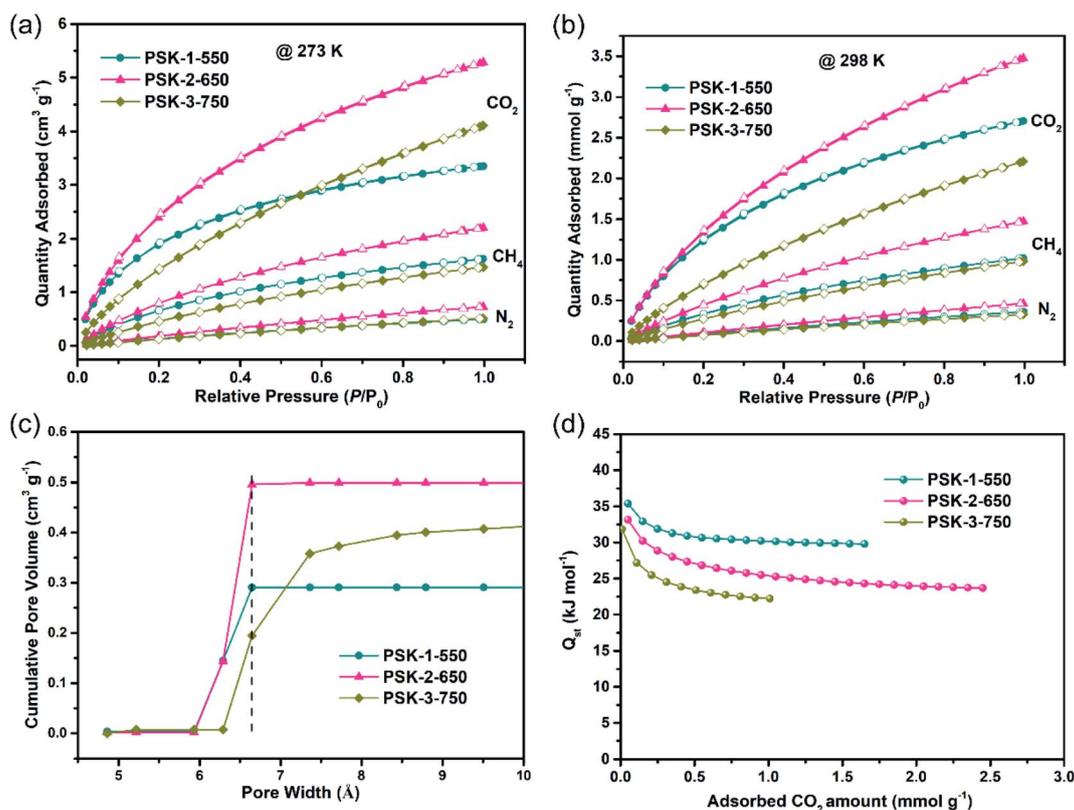

Fig. 3 CO_2, CH_4, N_2 adsorption isotherms (a) at 273 K and (b) at 298 K, (c) cumulative pore volume derived from N_2 adsorption at 77 K, (d) isoteric heat of CO_2 adsorption.

Å was contained in PSK-3-750. Moreover, the micropore volumes percentage of PSK-1-550 and PSK-2-650 are 66% and 76%, respectively. Whereas, the percentage decreased to 61% on PSK-3-750 (Table 1). The ratio of micropores is consistent with the conclusion obtained from the N_2 isotherm, which provides the theoretical basis for studying the influence of micropores on gas adsorption.

3.3 CO_2 adsorption features

By the virtue of the unique characteristics of large specific surface area and ultramicroporous structure of PS-derived porous carbon, these samples are expected to be highly efficient adsorbents for CO_2 capture and gas mixtures separation. CO_2, CH_4, and N_2 adsorption–desorption isotherms on the PS-derived porous carbon measured at 273, 298, and 323 K with pressure up to 1 bar are shown in Fig. 3a, b and S4–S6.† All isotherms fit well with the Langmuir–Freundlich model exhibit good reversibility without hysteresis, indicating that the adsorbed gas is easily desorbed by vacuum. PSK-2-650 exhibits the highest CO_2 uptake of being 5.28 and 3.48 mmol g^{-1} at 273 K and 298 K under 1 bar, which is higher than that of Chestnut-derived carbons (2.3 mmol g^{-1}),[33] Arundo donax derived carbon (2.2 mmol g^{-1}),[21] RLF-500 (3.13 mmol g^{-1}),[34] O-doped carbon adsorbents (3.46 mmol g^{-1})[35] at 298 K under 1 bar (Fig. 4a). The largest micropore volume of 0.35 cm g^{-1} and

highest microporous volume percentage (76%) was obtained on PSK-2-650 with neither the highest surface area nor hetero-atoms content. Thus, we can infer that ultra-micropores played a dominant role in CO_2 capture. The pore volume of narrow micropores followed the order of PSK-2-650 (0.36 cm^3 g^{-1}) > PSK-1-550 (0.24 cm^3 g^{-1}) > PSK-3-750 (0.12 cm^3 g^{-1}), which was consistent with the CO_2, CH_4 and N_2 capacity, this imply that the narrow micropores (<6.6 Å) play a dominate role in gas adsorption" (Fig. 3c). The CO_2 adsorption at 0.15 bar is analyzed because the CO_2 partial pressure in typical flue gas is this specific pressure. The highest CO_2 uptake amount at 0.15 bar and 273 K was 2.0 mmol g^{-1} obtained on PSK-2-650 as well, this value exceeded many reported adsorbents, such as peanut shell derived carbon (1.54 mmol g^{-1}),[22] *Camellia japonica* derived carbon (1.50 mmol g^{-1}),[36] *Paeonia lactiflora* and seaweed-derived porous carbon (1.30 mmol g^{-1}),[37] and N-doped carbon nanotubes (1.32 mmol g^{-1}).[38] In addition, the CH_4 uptake of PSK-2-650 is as high as 2.20 mmol g^{-1} at 273 K and 1.47 mmol g^{-1} at 298 K under 1 bar, which is comparable with SMOF-SIFSIX-1a (1.05 mmol g^{-1}),[39] M1273-150 (2.19 mmol g^{-1}),[40] and ClCTF-1-650 (2.20 mmol g^{-1})[41] at 1.0 bar under 273 K.

The isosteric heat of adsorption (Q_{st}) for PS-derived microporous carbons was calculated by the Clausius–Clapeyron equation based on the pure CO_2, CH_4, and N_2 isotherms (Fig. 3d and S7†).[42,43] The isosteric heat values of CO_2, CH_4 and N_2 in the initial stage are in the range of 22–39 kJ mol^{-1}, 21–31 kJ mol^{-1}
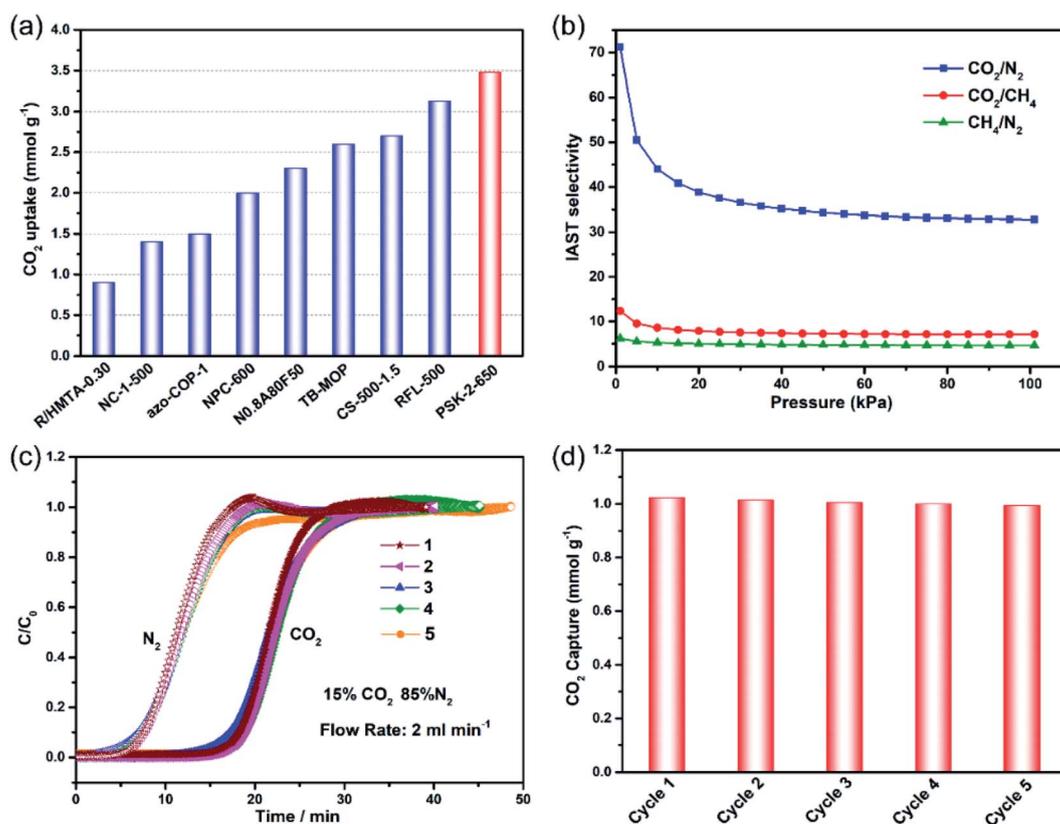

Fig. 4 (a) Comparison of CO_2 uptake among representative porous materials; (b) IAST selectivity of CO_2/N_2 (15 : 85), CO_2/CH_4 (10 : 90) and CH_4/N_2 (50 : 50) on PSK-1-550 at 298 K; (c) the breakthrough experiments of PSK-2-650 for CO_2/N_2 mixture (15/85, v/v) with a gas flow of 2 mL min^{-1}, (d) cyclic CO_2 adsorption capacity.

and 13–17 kJ mol^{-1} for the PS-derived carbons, which are located in the physisorption range. The high CO_2 adsorption heat is higher than polymers,[44] carbon adsorbents,[45,46] and MOFs.[47] The high Q_{st} at low surface coverage indicates that PS-derived carbons are promising adsorbents in the gas separations.

3.4 Gas separation selectivities

Considering the abundant ultra-micropores and high CO_2 uptake capacity, the carbon materials can act as preferential adsorbents for $CO_2/CH_4/N_2$ binary gas mixtures separation. Moreover, more CO_2 was adsorbed than CH_4 and N_2 due to higher quadrupole moment and polarizability of CO_2 molecule than that of CH_4 and N_2.[35,48] The selectivities of three binary gas pairs were calculated by the Ideal Adsorbed Solution Theory (IAST) based upon the single-component gas adsorption isotherms and the results were presented in Fig. S8† and Table 2. The gas pairs and proportions were designed according to flue gas (CO_2/N_2, 15 : 85), nature gas (CO_2/CH_4, 10 : 90), and coalbed gas (CH_4/N_2, 50 : 50), respectively. For CO_2/N_2 mixtures, the highest IAST selectivity was 32.7 obtained on PSK-1-550 at 298 K (Fig. 4b). The values is much higher than that of other reported adsorbents at 298 K under 1 bar, such as phenolic resin derived carbon (19),[49] Lotus stalk-derived carbon (16),[23] Bamboo derived carbon (8.6),[50] ordered mesoporous carbon (approximately 11.3),[51] and O-doped porous carbons (26.5).[35] The highest CO_2/CH_4 selectivity of 7.1 at 298 K and 1 bar was

obtained on PSK-1-550 as well (Fig. 4b), this value is also superior to other representative porous materials, such as silicalite-1 (2.6),[52] TP-MOP (4),[53] polyfuran-derived porous carbon (6.8),[54] and tar pitch derived porous carbons (1.7).[55] For CH_4/N_2 gas mixtures, the IAST selectivity is 4.6 obtained on PSK-1-550 at 298 K and 1 bar (Fig. 4b), which is also superior to PILCs (approximately 2),[56] nitrogen-doped porous carbon (3.6),[57] OMCs (3.7).[51] Given that the outstanding CO_2 capture and excellent gas separation performances, the PS-derived porous carbons are promising candidates in the selective CO_2 separation in real-world applications.

3.5 Breakthrough experiment and working capacity

To verify the real separation ability, PSK-2-650 was applied for the separation of several binary mixtures based on the breakthrough experiments. Gas mixtures of CO_2/N_2 (15/85), and CO_2/CH_4 (10/90) were applied to a packed column of PSK-2-650 at a flow rate of 2.0 mL min^{-1} and 298 K. The conditions and methods of the experiments in detail are described in the ESI.† For CO_2/N_2 (15 : 85) mixtures, N_2 eluted first through the column, then CO_2 was retained in the interior of the packed adsorbent for 11 min, and the dynamic separation factors were 2.0 based on the breakthrough experiment (Fig. 4c). The dynamic CO_2 uptake capacity was 1.01 mmol g^{-1} calculated from CO_2/N_2 (15 : 85) gas mixture. For CO_2/CH_4 (10 : 90) mixtures, the time interval between CO_2 and CH_4 is 6 min (Fig. S9†). What's more, the high-purity degree of CH_4 from biogas could be directly collected at a certain time.

Five successive cycles were conducted to confirm the multiple cycling and regeneration of PSK-2-650. The well-retained CO_2 capacity (Fig. 4d) and breakthrough time without any decay during five successive cycles indicate their outstanding stability and recyclability.

The potential of PS-derived carbons in CO_2 capture from flue gas (CO_2/N_2 = 15 : 85) was evaluated using vacuum swing adsorption (VSA) at 298 K. Five adsorption evaluation criteria, such as CO_2 uptake under adsorption conditions (N_1^{ads}), working CO_2 capacity (ΔN_1), regenerability (R), selectivity under adsorption conditions (α_{12}^{ads}), and the sorbent selection

Table 2 Isosteric adsorption heat of CO_2 and CH_4 and IAST selectivities of PS-derived carbons

| Sample | Q_{st} kJ mol^{-1} | | IAST selectivity (@298 K, 1 bar) | | |
	CO$_2$	CH$_4$	CO_2/N_2 (15 : 85)	CO_2/CH_4 (10 : 90)	CH_4/N_2 (50 : 50)
PSK-1-550	35.4	31.3	32.7	7.1	4.6
PSK-2-650	33.2	28.0	23.2	4.7	4.8
PSK-3-750	31.8	24.0	13.5	3.2	4.1

Table 3 Adsorbents for separation using vacuum swing adsorption (VSA) conditions (P_{ads} = 1 bar, P_{des} = 0.1 bar and T = 298 K)

Adsorbent	N_1^{adsc} (mmol g^{-1})	ΔN_1^d (mmol g^{-1})	R^e (%)	α_{12}^{adsf}	S^g	Reference
PSK-1-550[a]	1.02	0.81	79.4	32.7	94.9	This work
PSK-2-650[a]	1.09	0.89	81.7	23.2	57.5	This work
PSK-3-750[a]	0.55	0.47	85.5	13.5	24.7	This work
[Zn$_2$ (tcpb){p-(CF$_3$)NC$_5$H$_4$}$_2$][b]	0.16	0.13	80.7	43.9	57.9	48
BILP-10[b]	0.45	0.41	90.8	35.5	109.0	58
HKUST-1[b]	0.62	0.55	89.0	20.4	46.2	59
NoritR1 extra[b]	0.38	0.28	73.7	10.7	5.09	59
ZIF-81[b]	0.27	0.25	93.4	22.7	101	60
CNA[b]	0.43	0.42	98.0	113	427	61
SNU-Cl-va[b]	0.47	0.41	87.3	38	262	62

[a] Flue gas (CO_2/N_2 = 15 : 85). [b] Flue gas (CO_2/N_2 = 10 : 90). [c] N_1^{ads} (CO_2 uptake under adsorption conditions). [d] $\Delta N_1 = N_1^{ads} - N_1^{des}$ (CO_2 working capacity). [e] $R = \Delta N_1/N_1^{ads} \times 100$ (regenerability). [f] $\alpha_{12}^{ads} = (N_1^{ads}/N_2^{ads})/(y_2/y_1)$ IAST selectivity. [g] Sorbent selection parameter, $S = (\alpha_{12}^{ads})^2/(\alpha_{12}^{des})$ ($\Delta N_1/\Delta N_2$); selection parameter. 1: strongly adsorbed component (CO_2). 2: weakly adsorbed component (CH_4 or N_2). y: molar fraction in the equilibrium gas phase.

parameter (S) regarded as a comprehensive evaluation of sorbents as they provide insight into the trade-off between gas uptake and selectivity mentioned above.[58] Thus, the analysis can use the adsorption data of pure gas isotherms to help recognize promising adsorbents for gas separation under different industrial conditions (Table 3).[59] For CO_2/N_2 mixtures, PSK-2-650 with abundant ultra-micropores exhibit outstanding CO_2 uptake (1.09 mmol g^{-1}) at 298 K under 0.15 bar and result in a high CO_2 working capacity of 0.89 mmol g^{-1}. The working capacity exceeds most reported porous materials, such as BILP-10 (0.41 mmol g^{-1}), HKUST-1 (0.55 mmol g^{-1}), ZIF-81 (0.25 mmol g^{-1}) and CNA (0.42 mmol g^{-1}). What's more, the regenerability (R) of PSs are in the range of 79.4–85.5, which is also comparable to that of NoritR1 extra (73.4) and [Zn$_2$(tcpb){p-(CF$_3$)NC$_5$H$_4$}$_2$] (80.7). The outstanding selectivity factor ($\alpha_{12}^{ads} = 32.7$) of PSK-2-650 lead to its excellent sorbent selection parameter (S, 94.5), higher than that of HKUST-1 (46.2) and [Zn$_2$(tcpb){p-(CF$_3$)NC$_5$H$_4$}$_2$] (57.9), while slightly lower than BILP-10 (109) and ZIF-81(101). The five indicators mentioned above display that PSs have significant performance in CO_2 capture and separation in actual application.

4. Conclusion

In this study, novel palm sheath-derived carbonaceous adsorbents were prepared for CO_2 capture from two binary gas mixture pairs (CO_2/N_2, CO_2/CH_4). The obtained PS-derived carbons exhibit excellent CO_2 uptake and outstanding IAST selectivity at atmospheric pressure, which is significantly higher than most representative adsorbents ever reported. Detailed studies found that ultra-micropores are favorable for CO_2 capture under 1 bar. Moreover, the good results of breakthrough and regenerate experiments confirmed the excellent separation performance and recyclability. We further prove their superior CO_2 working capacity in VSA processes. This work illustrates the excellent selectivity, high gas adsorption capacity, good regeneration of PS-derived ultra-micropore carbons for challenging gas separation and thus will enlarge separation schemes in many actual applications.

Conflicts of interest

There are no conflicts to declare.

Acknowledgements

References

1 L. Lombardo, Y. Ko, K. Zhao, H. Yang and A. Züttel, *Angew. Chem., Int. Ed.*, 2021, **60**, 9580–9589.

2 S. Khodabakhshi, M. Taddei, J. A. Rudd, M. J. McPherson, Y. Niu, R. E. Palmer, A. R. Barron and E. Andreoli, *Carbon*, 2021, **173**, 989–1002.

3 M. L. Alcantara, G. De Almeida Oliveira, L. M. Lião, C. P. Borges and S. Mattedi, *Ind. Eng. Chem. Res.*, 2021, **60**, 4405–4419.

4 W. Tian, H. Zhang, H. Sun, A. Suvorova, M. Saunders, M. Tade and S. Wang, *Adv. Funct. Mater.*, 2016, **26**, 8651–8661.

5 A. Rehman, G. Nazir, K. Yop Rhee and S.-J. Park, *Chem. Eng. J.*, 2021, **420**, 130421.

6 F. Raganati, F. Miccio and P. Ammendola, *Energy Fuels*, 2021, **35**, 12845–12868.

7 J. G. Vitillo, B. Smit and L. Gagliardi, *Chem. Rev.*, 2017, **117**, 9521–9523.

8 B. Dutcher, M. Fan and A. G. Russell, *ACS Appl. Mater. Interfaces*, 2015, **7**, 2137–2148.

9 B. Yoon and G. S. Hwang, *Energy Fuels*, 2021, **35**, 16705–16712.

10 O. T. Qazvini, R. Babarao and S. G. Telfer, *Nat. Commun.*, 2021, **12**, 1–8.

11 Y. Zeng, R. Zou and Y. Zhao, *Adv. Mater.*, 2016, **28**, 2855–2873.

12 L. Wu, J. Liu, H. Shang, S. Li, J. Yang, L. Li and J. Li, *Microporous Mesoporous Mater.*, 2021, **316**, 110956.

13 Y. Belmabkhout, P. M. Bhatt, K. Adil, R. S. Pillai, A. Cadiau, A. Shkurenko, G. Maurin, G. Liu, W. J. Koros and M. Eddaoudi, *Nat. Energy*, 2018, **3**, 1059–1066.

14 S. Noro and T. Nakamura, *NPG Asia Mater.*, 2017, **9**, e433.

15 G. Singh, K. S. Lakhi, S. Sil, S. V. Bhosale, I. Y. Kim, K. Albahily and A. Vinu, *Carbon*, 2019, **148**, 164–186.

16 Y. Zhang, P. Zhang, W. Yu, J. Wang, Q. Deng, J. Yang, Z. Zeng, M. Xu and S. Deng, *Ind. Eng. Chem. Res.*, 2018, **57**, 14191–14201.

17 N. F. Attia, M. Jung, J. Park, H. Jang, K. Lee and H. Oh, *Chem. Eng. J.*, 2020, **379**, 122367.

18 H. Kim, J. Y. Jung, K. H. Park, P. Linga, Y. Seo and C. D. Wood, *Energy Fuels*, 2021, **35**, 13889–13899.

19 S. Xu, W. C. Li, C. T. Wang, L. Tang, G. P. Hao and A. H. Lu, *Angew. Chem., Int. Ed.*, 2021, **60**, 6339–6343.

20 A. S. González, M. G. Plaza, F. Rubiera and C. Pevida, *Chem. Eng. J.*, 2013, **230**, 456–465.

21 G. Singh, K. S. Lakhi, I. Y. Kim, S. Kim, P. Srivastava, R. Naidu and A. Vinu, *ACS Appl. Mater. Interfaces*, 2017, **9**, 29782–29793.

22 S. Deng, B. Hu, T. Chen, B. Wang, J. Huang, Y. Wang and G. Yu, *Adsorption*, 2015, **21**, 125–133.

23 P. Yang, L. Rao, W. Zhu, L. Wang, R. Ma, F. Chen, G. Lin and X. Hu, *Ind. Eng. Chem. Res.*, 2020, **59**, 6194–6201.

24 J. Li, K. Li, T. Zhang, S. Wang, Y. Jiang, Y. Bao and M. Tie, *Fibers Polym.*, 2016, **17**, 880–887.

25 T. Wei, Q. Zhang, X. Wei, Y. Gao and H. Li, *Sci. Rep.*, 2016, **6**, 22646.

26 R. Wang, P. Wang, X. Yan, J. Lang, C. Peng and Q. Xue, *ACS Appl. Mater. Interfaces*, 2012, **4**, 5800–5806.

27 A. C. Ferrari and J. Robertson, *Phys. Rev. B: Condens. Matter Mater. Phys.*, 2001, **64**, 075414.

28 J. H. Kaufman, S. Metin and D. D. Saperstein, *Phys. Rev. B: Condens. Matter Mater. Phys.*, 1989, **39**, 13053–13060.

29 T. Lin, I.-W. Chen, F. Liu, C. Yang, H. Bi, F. Xu and F. Huang, *Science*, 2015, **350**, 1508–1513.

30 P. Schneider, *Appl. Catal., A*, 1995, **129**, 157–165.

31 C. Zhang, W. Song, Q. Ma, L. Xie, X. Zhang and H. Guo, *Energy Fuels*, 2016, **30**, 4181–4190.

32 X. Ren, H. Li, J. Chen, L. Wei, A. Modak, H. Yang and Q. Yang, *Carbon*, 2017, **114**, 473–481.

33 K. M. Nelson, S. M. Mahurin, R. T. Mayes, B. Williamson, C. M. Teague, A. J. Binder, L. Baggetto, G. M. Veith and S. Dai, *Microporous Mesoporous Mater.*, 2016, **222**, 94–103.

34 G. P. Hao, W. C. Li, D. Qian and A. H. Lu, *Adv. Mater.*, 2010, **22**, 853–857.

35 J. Wang, R. Krishna, J. Yang and S. Deng, *Environ. Sci. Technol.*, 2015, **49**, 9364–9373.

36 H. M. Coromina, D. A. Walsh and R. Mokaya, *J. Mater. Chem. A*, 2016, **4**, 280–289.

37 N. Balahmar, A. S. Al-Jumialy and R. Mokaya, *J. Mater. Chem. A*, 2017, **5**, 12330–12339.

38 Q. Cen, M. Fang, T. Wang, I. Majchrzak-Kucęba, D. Wawrzyńczak and Z. Luo, *Greenhouse Gases: Sci. Technol.*, 2016, **6**, 787–796.

39 J. Dai, D. Xie, Y. Liu, Z. Zhang, Y. Yang, Q. Yang, Q. Ren and Z. Bao, *Ind. Eng. Chem. Res.*, 2020, **59**, 7866–7874.

40 Y. Li, D. Li, Y. Rao, X. Zhao and M. Wu, *Carbon*, 2016, **105**, 454–462.

41 J. Wang, J. Yang, R. Krishna, T. Yang and S. Deng, *J. Mater. Chem. A*, 2016, **4**, 19095–19106.

42 J. Wang, L. Huang, R. Yang, Z. Zhang, J. Wu, Y. Gao, Q. Wang, D. O'Hare and Z. Zhong, *Energy Environ. Sci.*, 2014, **7**, 3478–3518.

43 Y. Li, B. Zou, C. Hu and M. Cao, *Carbon*, 2016, **99**, 79–89.

44 J. Duan, M. Higuchi, J. Zheng, S. I. Noro, I. Y. Chang, K. Hyeon-Deuk, S. Mathew, S. Kusaka, E. Sivaniah, R. Matsuda, S. Sakaki and S. Kitagawa, *J. Am. Chem. Soc.*, 2017, **139**, 11576–11583.

45 L. Guo, J. Yang, G. Hu, X. Hu, L. Wang, Y. Dong, H. Dacosta and M. Fan, *ACS Sustainable Chem. Eng.*, 2016, **4**, 2806–2813.

46 D. Qian, C. Lei, E. M. Wang, W. C. Li and A. H. Lu, *ChemSusChem*, 2014, **7**, 291–298.

47 S. Saha, S. Chandra, B. Garai and R. Banerjee, *Indian J. Chem., Sect. A: Inorg., Bio-inorg., Phys., Theor. Anal. Chem.*, 2012, **51**, 1223–1230.

48 Y.-S. Bae, O. K. Farha, J. T. Hupp and R. Q. Snurr, *J. Mater. Chem.*, 2009, **19**, 2131.

49 S. Liu, L. Rao, P. Yang, X. Wang, L. Wang, R. Ma, L. Yue and X. Hu, *J. Environ. Sci.*, 2020, **93**, 109–116.

50 H. Wei, S. Deng, B. Hu, Z. Chen, B. Wang, J. Huang and G. Yu, *ChemSusChem*, 2012, **5**, 2354–2360.

51 B. Yuan, X. Wu, Y. Chen, J. Huang, H. Luo and S. Deng, *Environ. Sci. Technol.*, 2013, **47**, 5474–5480.

52 J. Yang, J. Li, W. Wang, L. Li and J. Li, *Ind. Eng. Chem. Res.*, 2013, **52**, 17856–17864.

53 H. Hong, Z. Guo, D. Yan and H. Zhan, *Microporous Mesoporous Mater.*, 2020, **294**, 109870.

54 J. Wang, R. Krishna, X. Wu, Y. Sun and S. Deng, *Langmuir*, 2015, **31**, 9845–9852.

55 A. Arami-Niya, T. E. Rufford and Z. Zhu, *Carbon*, 2016, **103**, 115–124.

56 J. Pires, V. K. Saini and M. L. Pinto, *Environ. Sci. Technol.*, 2008, **42**, 8727–8732.

57 J. Wang, R. Krishna, J. Yang, K. P. R. Dandamudi and S. Deng, *Mater. Today Commun.*, 2015, **4**, 156–165.

58 A. K. Sekizkardes, T. Islamoğlu, Z. Kahveci and H. M. El-Kaderi, *J. Mater. Chem. A*, 2014, **2**, 12492–12500.

59 Y. S. Bae and R. Q. Snurr, *Angew. Chem., Int. Ed.*, 2011, **50**, 11586–11596.

60 R. Banerjee, H. Furukawa, D. Britt, C. Knobler, M. O. Keeffe and O. M. Yaghi, *J. Am. Chem. Soc.*, 2009, **131**, 3875–3877.

61 Y. Oh, V. D. Le, U. N. Maiti, J. O. Hwang, W. J. Park, J. Lim, K. E. Lee, Y. S. Bae, Y. H. Kim and S. O. Kim, *ACS Nano*, 2015, **9**, 9148–9157.

62 B. Ashourirad, P. Arab, T. Islamoglu, K. A. Cychosz, M. Thommes and H. M. El-Kaderi, *J. Mater. Chem. A*, 2016, **4**, 14693–14702.